Available online at www.sciencedirect.com
SCIENCE DIRECT®
Polymer 44 (2003) 3985–3994
polymer
www.elsevier.com/locate/polymer

Effects of soft-segment prepolymer functionality on structure–property relations in RIM copolyurethanes

John L. Stanford[a], Richard H. Still[a], Arthur N. Wilkinson[b,*]

[a]*Manchester Materials Science Centre, University of Manchester and UMIST, Grosvenor Street, Manchester M1 7HS, UK*
[b]*Department of Chemistry and Materials, Manchester Metropolitan University, John Dalton Building, Chester Street, Manchester M1 5GD, UK*

Received 11 July 2002; received in revised form 4 April 2003; accepted 15 April 2003

Abstract

Segmented copolyurethanes comprising 40–60% by weight of polyurethane hard segments (HS) and polyether soft-segment (SS) with different functionalities (SS-f_n), have been formed by reaction injection moulding (RIM). The HS were formed from 4,4′ diphenylmethane diisocyanate (MDI) reacted with ethane diol (ED). The three SS-prepolymers used were all hydroxyl-functionalised poly(oxypropylene-*b*-oxyethylene)s with different nominal functionalities (f_n) of 2, 3 and 4 but with a constant molar mass per functional group of ~2000 g mol^{-1}. RIM materials were characterised using differential scanning calorimetry, dynamic mechanical thermal analysis, tensile stress–strain and single-edge notch fracture studies. Predictions using a statistical model of the RIM-copolymerisation showed that increasing SS-f_n lead to more rapid development of copolymer molar mass with isocyanate conversion. Experimentally, the RIM-PU exhibited a wide range of mechanical behaviour resulting from differences in molecular and morphological structures. Increasing SS-f_n produced materials with improved mould release behaviour and fracture resistance. However, increasing SS-f_n also reduced the degree of phase separation developed in the copolyurethanes, resulting in increased modulus–temperature dependence and poorer tensile properties.

Keywords: Reaction injection moulding; Polyurethanes; Phase separation

1. Introduction

Copoly(urethane)s (PU) formed by reaction injection moulding (RIM) [1] are used extensively to produce elastomeric components. In general terms, RIM-PU are regarded as segmented block copolymers, formed via random-step reactions of mixtures of hydroxyl-functionalised polyethers and aliphatic diols with aromatic diisocyanates. However, during reaction to form the copolymers, as the liquid reactants are rapidly converted to a solid, a combination of spinodal decomposition-induced phase separation [2,3] and solidification of the hard segments (due to crystallisation or vitrification) effectively quenches the system to yield a mixture of reaction products comprising homopolymers, various AB-type block copolymers and free monomers [4]. This solid mixture possesses a non-equilibrium morphology comprising co-continuous, soft- and hard-segment phases, the degree of phase separation of which depends on hard-segment (HS) content, thermal history and hard-segment structure [5–7]. The effects of soft-segment (SS) prepolymer molecular structure on phase separation [8] are highly significant in determining copolymer morphology and properties. Varying the chemical structure of the SS changes its solubility parameter [9,10] and hence compatibility between soft and hard segments. In addition, increasing SS-prepolymer molar mass at constant functionality (i.e. increasing the molar mass per functional group or equivalent weight, E_n) results [11–14] in a higher degree of phase separation again due to increased incompatibility between the two copolymer segments. However, the effects on RIM-copolymers of varying the functionality of the SS-prepolymer (SS-f_n) at constant equivalent weight have been investigated for amine-based systems only [15–18]. In general, these studies indicate that increased SS-f_n results in reduced mould residence (or 'cure') time prior to demoulding and higher 'green strength' upon demoulding, but reduced flow-path length prior to solidification, or 'flowability' [15]. These changes have been linked to a more rapid development of

* Corresponding author.
E-mail address: a.wilkinson@mmu.ac.uk (A.N. Wilkinson).

0032-3861/03/$ - see front matter © 2003 Elsevier Science Ltd. All rights reserved.
doi:10.1016/S0032-3861(03)00357-4

copolymer molar mass with increasing SS-f_n via a statistical model of the RIM-copolymerisation [18]. Soft-segment prepolymers utilised in RIM-PU are usually di- or tri-functional polyoxypropylenes with equivalent weights in the range 1000–2000 g mol^{-1} which, in order to increase their reactivity, are endcapped with 10–25% of polyoxyethylene to give primary-hydroxyl tipped polyols. This paper reports on the effects of varying the functionality of SS-prepolymers, with constant E_n, on the structural development of RIM-PU. The resulting variations in copolymer molar mass and microphase separation, and their effects on thermal and mechanical properties, are presented.

2. Experimental

2.1. Reactants

The materials formed in this study comprised up to four components: (i) a polyisocyanate, (ii) a polyether prepolymer with $E_n \approx 2000$ g mol^{-1}, (iii) ethane diol chain extender, and (iv) a catalyst for the hydroxyl-isocyanate reaction. The chemical structures of the various reactants are shown in Scheme 1.

The polyisocyanate, (**I**), Isonate M340 (ex. Dow Chemical), is a mixed uretonimine/ urethane modified variant of 4,4′-diphenylmethane diisocyanate (MDI) with a value of $E_n = 161 \pm 1.5$ g mol^{-1} by isocyanate titration, and a nominal functionality of 2.15. The three polyethers are poly(oxypropylene-b-oxyethylene)s, (**II**), DS25 diol, M1 triol and P1 tetrol. These polyols are block copolymers comprising ~80–85 mol% of oxypropylene end-capped with ~20–15 mol% of oxyethylene. The E_n of each of the prepolymers was determined by acetylation, and GPC was used to determine mean molar masses relative to polyoxyethylene standards. The aliphatic diol chain extender, ethane diol (ED), (**III**), was stored over molecular sieves prior to processing. The RIM-PU systems contained a synergistic catalyst mixture of triethylene diamine (TEDA) and dibutyltin-dilaurate (DBTDL) [19] at constant concentrations relative to the overall hydroxyl concentration of 0.254 and 0.114 parts per OH equivalent, respectively. All reactants were used as-received without further purification.

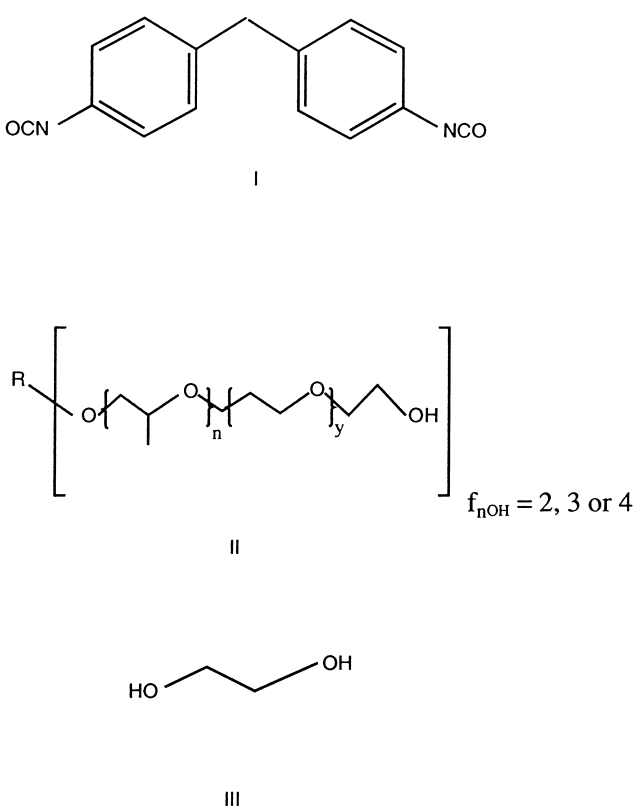

Scheme 1.

2.2. Reaction injection moulding

RIM materials were moulded as rectangular plaques (200 × 250 × 3.5 mm^3) using in-house RIM equipment that has been described in detail elsewhere [20]. The formulations and processing data are given in Table 1, where Q_i and Q_p are the machine throughputs used, respectively, for the polyisocyanate and the polyol reactant streams, η_p and Re_p are the viscosity and the Reynolds number of the polyol reactant stream. The materials were formulated to contain 40, 50 or 60% by weight ED/MDI hard segments, and the stoichiometric ratio of isocyanate to total hydroxyl groups used was 1.03. Reactant pressures of 3000 ± 50 psi, a mould temperature of 70 ± 1 °C, demould time of 5 min and initial reactant temperatures of 35 and 40 °C, for the polyisocyanate and polyol respectively, were used throughout. In order to achieve efficient impingement mixing of the reactants a critical value of Reynolds Number (Re) must be exceeded by the polyol stream, as this has the highest viscosity. The values of Re for the polyol stream (Re_p) in Table 1 all exceed the critical values of Re quoted in the literature [1], which vary between 50 and 250 for PU-systems. Plaques for testing were demoulded after 10 min. The materials produced are designated using a four-character code referring to the SS-prepolymer used and the HS content. For example, DS50 is a copoly(urethane) of 50% HS content formed using the polyether diol DS25.

2.3. Differential scanning calorimetry (DSC)

DSC phase separation studies were performed on a DuPont 990 Thermal Analyser fitted with a DuPont 910 cell base, equipped with a 990 DSC cell. Samples (10–15 mg) and an inert reference material, 10 mesh glass beads (~10 mg), were encapsulated in aluminium pans and cooled rapidly to −120 °C in the cell. The sample and reference were subjected to a 20 °C min^{-1} heating rate in static air to 50 °C. The glass transition temperatures were obtained from the DSC trace as the intersection of tangents

Table 1
Formulations and processing parameters used to produce RIM-PU

Formulation	D40	D50	D60	M40	M50	M60	P40	P50	P60
Prepolymer[a]	100	100	100	100	100	100	100	100	100
M340[a]	71.7	102.3	148.2	70.0	101.2	146.8	70.3	100.5	146.1
ED[a]	11.5	17.0	25.5	11.3	16.9	25.4	11.3	17.0	25.3
Q_i (g s^{-1})	80.1	96.0	129.7	78.7	92.4	167.1	77.3	90.1	143.5
Q_p (g s^{-1})	122.5	110.5	110.7	124.3	107.4	100.5	122.7	105.4	124.0
η_p (Pa s)[b]	0.33	0.33	0.33	0.40	0.39	0.39	0.48	0.47	0.47
Re_p	1035	893	893	782	745	721	647	613	664

[a] Parts by weight.
[b] Viscosity values were obtained at 50 °C which includes the temperature rise (11 ± 2 °C) in the reactant stream arising from viscous dissipation [20].

drawn to the onset baseline and the endothermic slope. The degree of phase separation for each copolymer studied was obtained using the method of Camberlin and Pascault [21]. Thus the heat capacity change, ΔC_p^S, at the soft segment glass transition, T_g^S, was measured and compared to ΔC_p^{SO}, the heat capacity change of the pure soft segment material. The hard segment fraction of the material was known and the phase separation ratio (PSR) was determined as reported previously [5,6,18].

2.4. Dynamic mechanical thermal analysis (DMTA)

DMTA data were obtained in the range − 100 to 300 °C using a Polymer Laboratories apparatus operating at a frequency of 1 Hz and a heating rate of 5 °C min^{-1}. A double cantilever bending geometry was used for beam samples ($3 \times 10 \times 45$ mm^3) to obtain dynamic flexural moduli and mechanical damping as functions of temperature.

2.5. Tensile stress–strain

Tensile stress–strain data were obtained at 20 ± 2 °C using an Instron 1122 universal testing machine, with dumb-bell specimens having an overall length of 150 mm, neck length of 50 mm, width of 12.5 mm and thickness of 3.5 mm. The crosshead separation gauge length was 75 mm and the extension rate 10 mm min^{-1}. The strain in the sample up to 10% was recorded using a strain-gauge extensometer clamped directly to the neck of the specimen. Typically, 10 specimens were tested for each material and the derived tensile properties are reported as the mean of at least eight tests.

2.6. Single edge notch fracture measurements

The fracture properties of the RIM-copolymers were measured in a single edge-notch tensile (SENT) geometry using rectangular specimens of length 150 mm, width (d) 25 mm and thickness (b) 3.5 mm. Tests were conducted at 20 ± 2 °C using an Instron 1122 universal testing machine at an extension rate of 10 mm min^{-1} and a specimen gauge length of 75 mm. At least 20 specimens were tested for each material and the nominal notch depth, a, was varied to give a/d ratios in the range $0.04 \leq a/d \leq 0.5$. Notches were cut approximately to pre-determined depths using a saw and finished with a fresh razor blade to sharpen the notch. During the tests, the onset of crack propagation was determined visually and marked on the force–time curve. After fracture, notch depths were measured accurately to ±0.001 mm using a travelling microscope.

3. Results and discussion

3.1. Characterisation of reactants

The values of E_n in Table 2 obtained from acetylation are similar for the various prepolymers, varying between ~2050 and ~2300 g mol^{-1}. Typically, end-capped polyols of the type used contain primary and secondary hydroxyl groups, with ~80% being primary [1,22,23]. The number-average functionalities (f_n) of the polyols were determined from the ratio of number-average molar mass (from GPC) to equivalent weight, and are given in the last column of Table 2. In the case of the triol and tetrol, the values of f_n, are lower than the nominal values, 3 and 4, respectively. These differences are due to side reactions that occur during the base-catalysed propoxylation [22,24] process used to produce the polyols, yielding unreactive, unsaturated end groups.

3.2. Reaction injection moulding

Preliminary experimentation showed that systems based

Table 2
Characterisation data for soft segment prepolymers

Prepolymer	E_n (g mol^{-1})[a]	M_n (g mol^{-1})[b]	f_n[c]
DS25 diol	2046 ± 19	4206	2.06
M1 triol	2182 ± 22	6066	2.78
P1 tetrol	2287 ± 23	7982	3.49

[a] E_n, number-average molar mass per functional group from acetylation.
[b] Number-average molar mass from GPC.
[c] Number-average functionality [$f_n = M_n$(GPC)/E_n(acetylation)].

on M1 triol and P1 tetrol could be moulded with relatively low levels of additional catalyst at demould times of ≤ 3 min. However, the DS25-based systems required either increased catalyst levels or higher mould temperatures (>70 °C) to be moulded successfully, otherwise the surface of the mould cavity became fouled with a powdery film which had detached from the surface of the mouldings. In order to eliminate this problem, and hence produce good quality mouldings from all the RIM-PU systems using the chosen conditions of a demould time of 5 min at a mould temperature of 70 °C, it was found necessary to use the TEDA/DBTDL catalyst system at a concentration of 0.254 and 0.114 parts per OH equivalent, respectively. Similar powdery surface films have been observed on linear RIM-PU mouldings moulded at 70 °C and containing relatively low catalyst concentrations [25,26]. GPC analysis showed these films to consist of a mixture of very low molar mass polymer and oligomers, but substitution of the diol prepolymer with a triol prepolymer of the same equivalent weight eliminated the problem [25,26]. These surface films are the result of the layer of the copolymerising mixture immediately adjacent to the cavity wall undergoing 'premature' phase separation and vitrification, i.e. at a low degree of conversion. Therefore, increasing either the catalyst concentration or the functionality of the SS-prepolymer effectively increases the rate of copolymerisation relative to the rate of phase separation and will produce surface layers with higher molar mass and superior mechanical properties.

3.3. Differential scanning calorimetry, DSC

For all the RIM-PU endothermic base-line deviations ascribed to SS glass transitions at temperatures T_g^S were observed at approximately -65 ± 3 °C. The DSC data presented in Table 3 show the trend in T_g^S values on progressing from unreacted prepolymers to isolated SS-networks to phase separated copolymers. The table also allows comparison of the effects on T_g^S and PSR data of both the SS-prepolymer functionality and the HS%.

Reacting the SS-prepolymers with M340 polyisocyanate to form an isolated polyether network results in a rise in T_g^S of ~ 5 °C. This results from restrictions to molecular mobility of units at the ends of soft segment chains upon being incorporated into the network. Comparing the values of T_g^S of the networks with those of the RIM-copolymers, only small increases ($\sim 3 \pm 1$ °C) are observed indicating that the SS-phase responsible for the transition is relatively pure. In general, the value of T_g^S for both the SS-prepolymers and RIM-copolymers increased by ~ 4 °C upon increasing the nominal SS-prepolymer functionality from 2 to 3. This increase is indicative of a restriction of molecular mobility with increasing functionality, but a further increase in functionality to 4 (P1 polyol) had no significant effect upon values of T_g^S.

In Table 3, the value of PSR for each material is given as

Table 3
T_g^S and phase separation data for RIM-PU from DSC

	T_g^S (°C)	PSR (%)
Copolymers		
D40	−68	82 ± 4
D50	−67	66 ± 3
D60	−66	65 ± 4
M40	−63	64 ± 3
M50	−63	61 ± 3
M60	−62	59 ± 5
P40	−64	50 ± 3
P50	−64	48 ± 2
P60	−62	46 ± 3
Networks		
M1/M340	−66	–
P1/M340	−65	–
Prepolymers		
DS25	−74	–
M1	−70	–
P1	−70	–

T_g^S derived from at least three traces for each material, typical 95% confidence limits(CL) ± 1 °C. PSR data are averaged from at least nine determinations for each material and are shown ±95% CL.

the ratio of the heat capacity change of a RIM-copolymer at T_g^S compared to that of the pure SS-network, normalised for sample mass. The value of PSR is a measure of the fraction of SS which contributes to heat capacity at T_g^S and therefore does not include SS trapped either in the HS phase or the interfacial regions. The data in Table 3 show that all the RIM-PU show a general reduction in PSR as HS content is increased, in particular for the DS25 diol based system. This reduction in the degree of phase separation is in agreement with previously reported PSR data for RIM copolymers [5–7,18] but is contrary to thermodynamic predictions [5,21] based on calculations of χ_{HS}/χ_C^L; the ratio of the hard segment/soft segment interaction parameter (derived from their solubility parameters [10]) to the critical interaction parameter, χ_C^L, for the occurrence of microphase separation in a segmented block copolymer system [27,28]. Thus, theory predicts that the longer HS-sequence lengths formed at higher HS contents should result in higher degrees of microphase separation. This disagreement between prediction and experiment can be ascribed to the dynamic nature of the RIM process in which the onset of microphase separation occurs at a relatively early stage of the copolymerisation [3,29,30].

The value of PSR is observed to decrease significantly with both increasing HS-content and increasing SS-prepolymer functionality. As HS-content is increased both microphase separation and HS-solidification occur at an earlier stage of the copolymerisation, resulting in the formation of increasingly complex mixtures of monomers, homopolymers and various AB-type block copolymers of relatively low molar mass which exhibit a higher degree of phase-mixing. The decrease in PSR with SS-f_n may be ascribed to the more rapid development of molar mass during copolymerisation. The concomitant reduction in

molecular mobility within the system will slow the rate of phase separation, relative to the rate of polymerisation, and thus the system will be more phase-mixed at the onset of HS-solidification.

3.4. Dynamic mechanical thermal analysis

The curves in Figs. 1 and 2 show storage modulus (E') and damping (tan δ) versus temperature data for the RIM-PU materials. These curves are similar to those reported previously [14,31] for analogous phase-separated RIM-copolyurethanes, in that two major transitions are observed ascribed to the SS and HS glass transitions at temperatures T_g^S at approximately $-40\,^{\circ}C$ and T_g^H at approximately 130 °C. In addition, the damping curves show a broad, low intensity mixed-phase transition between 50 and 100 °C, which is associated with the breakdown of hydrogen bonding between HS urethane groups and the ether-oxygens

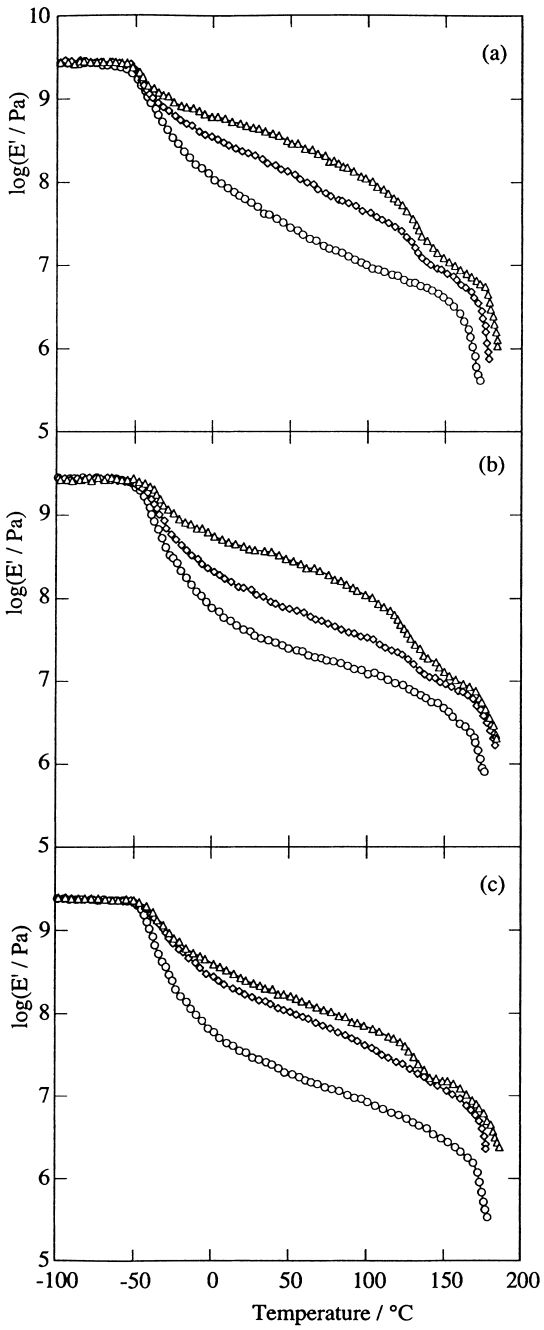

Fig. 1. Dynamic flexural modulus (E') at 1 Hz versus temperature for copolyurethanes; (a) DS25-based, (b) M1-based and (c) P1-based. For each group of RIM-PU their HS contents are indicated by the symbols used: i.e. 40% (circle), 50% (diamond) and 60% (triangle).

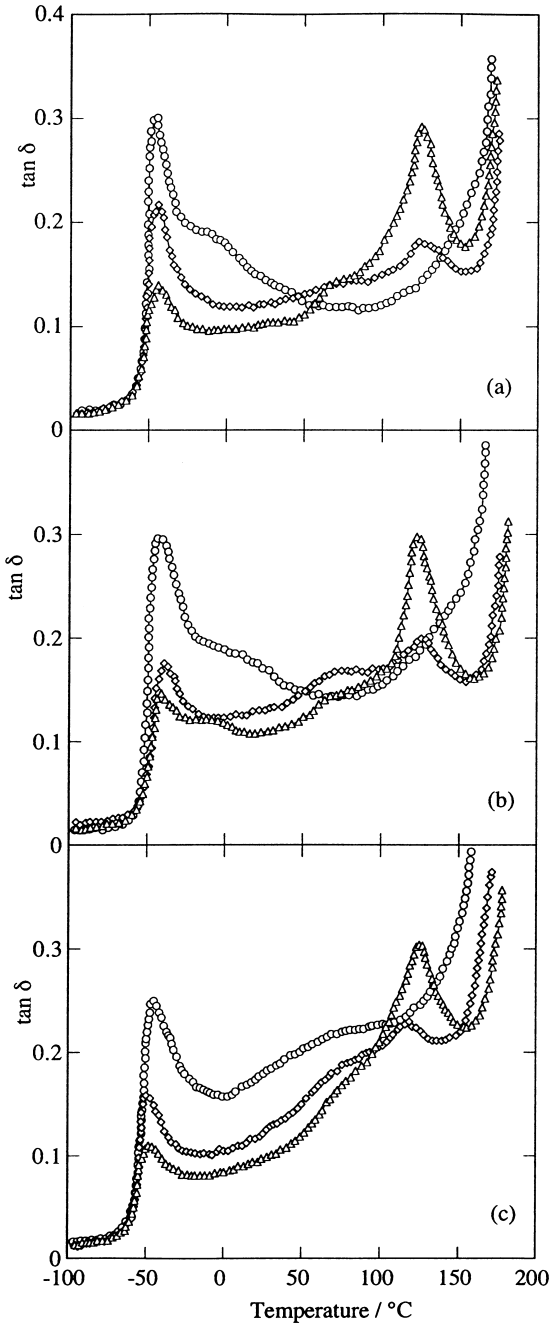

Fig. 2. Mechanical damping (tan δ) at 1 Hz versus temperature for copolyurethanes. (a) DS25-based, (b) M1-based and (c) P1-based. For each group of RIM-PU their HS contents are indicated by the symbols used: i.e. 40% (circle), 50% (diamond) and 60% (triangle).

of the SS. Detailed differences in values of T_g^S, T_g^H for the various PU are given in Table 4.

The mechanical damping data show the value of T_g^S (-39 ± 3°C) to be relatively insensitive to variations in SS-f_n, and in reasonable agreement with DMTA values of T_g^S of -40 ± 1 °C for homogeneous polyurethane networks derived from M340 and either M1 or P1 [32]. These observations indicate that the SS-phases responsible for the low temperature damping peaks are relatively pure. However, in some of the materials the temperature range of the transition region is significantly broader (approximately -60 to $+45$ °C) than the range -60 to 0 °C exhibited by the M1- and P1-based networks indicating a significant degree of domain boundary mixing. The degree of phase mixing was observed to increase slightly with HS-content, as evidenced by a small increase in T_g^S and a broadening of the transition peak, resulting from the onset of HS vitrification at a lower degree of phase separation. These broad transitions are therefore artefacts of the rapid solidification of the system at a relatively early stage of the microphase separation process. The width of these transitions also results in larger differences in the values of T_g^S measured by DSC (Table 3) and DMTA (Table 4), than the typical 10–15 °C difference exhibited by a block copolymer synthesised in a relatively slow copolymerisation.

More significant differences between the RIM-PU systems are observed for values of T_g^H. The 40% HS materials exhibit no obvious glass transition only a rising tan δ curve at temperatures >100 °C, whereas the 50 and 60% HS materials exhibit definite transition peaks at temperatures ~ 130 °C, suggesting the presence of longer HS sequence lengths in these materials. However as with T_g^S, the value of T_g^H (126 ± 3°C) is relatively insensitive to variations in SS functionality.

The modulus–temperature dependence of the various RIM-PU, expressed as the ratio of moduli at specified temperatures, is also given in Table 4. The ratio of moduli at -30 and 65 °C is often quoted [1] as an indicator of the low temperature modulus–temperature behaviour of RIM-copolymers. The magnitude of this ratio is dominated by the modulus change associated with the SS glass transition, the proximity of T_g^S to -30 °C and the degree of phase mixing present in the material. In this case, the modulus–temperature behaviour of the RIM-PU is dominated by HS-content, such that the modulus ratio increases in the order 40% HS > 50% > 60% (Table 4). Modulus–temperature behaviour at higher temperatures is quantified over an equal temperature interval by the modulus ratio $E'(65\ °C)/E'(160\ °C)$. When compared to the values of $E'(-30\ °C)/E'(65\ °C)$ the higher temperature ratio data exhibit not only a strong correlation with HS-content, although now 40% < 50% < 60% due to increasing the content of the higher softening HS, but also reduced modulus–temperature dependence at higher SS-f_n, possibly as a result of increased copolymer molar mass.

3.5. Tensile stress–strain

The tensile properties of the RIM-PU in terms of Young's modulus (E), yield and ultimate stresses (σ_y and σ_u), yield and ultimate strains (ε_y and ε_u) and tensile toughness (U_t, the total area under a stress–strain curve) have been derived from averaged stress–strain curves (at least five determinations for each material) and are summarised in Table 5. To aid discussion, the stress–strain curves in Fig. 3(a)–(c) are presented as stress versus log extension ratio. This has the effect of expanding the initial portion of the curves relative to engineering stress–strain curves.

There are two characteristic regions to the stress–strain curves. At low strains the materials have a high modulus and the slope of the stress–strain curve is very steep. All the materials display extrinsic yield points followed by extensive post-yield drawing with a much shallower increase in the stress–strain curve. This tensile behaviour been interpreted [33] as being indicative of materials with a bicontinuous morphology, with the initial part of the curve being attributed to deformation and yielding of the

Table 4
Data from DMTA for RIM-copolymers

Copolymer	γ^a		β^b	α^c		$E'(-30\ °C)/E'(65\ °C)$	$E'(65\ °C)/E'(160\ °C)$
	(°C)	tan δ	(°C)	(°C)	tan δ		
D40	−41	0.304	–	–		19.0	7.9
D50	−42	0.216	50–90	129	0.180	8.2	14.3
D60	−42	0.141	60–100	127	0.294	4.9	25.9
M40	−36	0.293	–	–		21.3	7.9
M50	−37	0.169	50–100	129	0.209	11.3	8.5
M60	−38	0.139	50–100	127	0.293	8.9	21.2
P40	−37	0.254	20–100	–		18.8	6.5
P50	−38	0.143	50–100	123	0.210	11.3	7.3
P60	−39	0.110	50–80	127	0.302	5.9	13.3

[a] Ascribed to the soft-segment glass transition at temperature T_g^S.
[b] Ascribed to a mixed-phase transition.
[c] Ascribed to the hard-segment glass transition at temperature T_g^H.

Table 5
Tensile stress–strain and SENT fracture properties of RIM-PU

Copolymer	E (MPa)	σ_u (MPa)	ε_u (%)	U_t (MJ m^{-3})	G_{IC} (kJ m^{-2})	σ_y[a] (MPa)	b_{min}[b] (mm)
D40	36 ± 2	10.7 ± 0.3	416 ± 12	43 ± 1	1.3 ± 0.2	3.6	9.6
D50	157 ± 5	22.9 ± 1.3	363 ± 17	73 ± 3	2.3 ± 0.2	6.8	19.9
D60	339 ± 11	26.2 ± 1.2	192 ± 10	62 ± 3	3.2 ± 0.3	11.6	20.1
M40	33 ± 2	9.0 ± 1.0	345 ± 43	32 ± 1	0.6 ± 0.1	3.4	4.3
M50	131 ± 8	22.1 ± 2.3	305 ± 16	58 ± 1	3.0 ± 0.3	5.3	35.0
M60	290 ± 15	21.6 ± 1.4	169 ± 7	40 ± 1	4.7 ± 0.4	9.6	36.9
P40	27 ± 2	8.4 ± 0.4	344 ± 21	31 ± 1	0.9 ± 0.1	2.1	13.7
P50	116 ± 7	19.2 ± 2.1	296 ± 21	52 ± 2	4.4 ± 0.3	4.5	63.1
P60	234 ± 17	19.4 ± 0.8	135 ± 11	27 ± 1	6.7 ± 0.6	6.8	85.0

Data are shown as mean values ± 95% confidence limits.
[a] Determined from extrinsic yield points of averaged curves using Considere's construction.
[b] Thickness criterion calculated from Eq. (2).

continuous hard-segment phase whilst the extensive post-yield drawing results from deformation of the rubbery soft-segment phase.

The data in Table 5 show the tensile behaviour of the RIM-PU to be dominated by HS-content. Thus, increasing the weight fraction of the rigid HS from 40 to 60% results in increases in modulus, yield stress and ultimate stress, but reductions in ultimate elongation. Consequently, tensile toughness values exhibited maxima at 50% HS-content. In general, the effect of increasing SS-f_n was to decrease all the tensile properties measured for the RIM-PU. These reductions in properties may be related to the decrease in the degree of phase separation upon increasing SS-f_n, as outlined by the PSR data. Thus, E and σ_u will fall as a smaller proportion of the hard segments are located in the reinforcing hard phase, and the presence of phase-mixed hard segments will inhibit the elastomeric nature of the soft-phase, thus reducing ε_u.

3.6. Single edge notch fracture measurements

All the RIM-copolymers in the present study exhibited bulk, non-linear elastic behaviour during the SENT tests and their fracture behaviour was therefore analysed using a tearing analysis [34] to determine the critical strain–energy release rate, G_{Ic}, or fracture energy.

The G_{Ic} is defined for the test geometry used by the relation [34]:

$$G_{Ic} = 2kW_c a \quad (1)$$

where a is the initial crack length, W_c is the strain–energy density of the specimen (determined from the integrated area under the stress–strain curve between zero deflection and the point of crack propagation) and k is a strain-dependent constant. An approximate expression for k has been derived [35] as $k = \pi/\lambda_c^{1/2}$ where λ_c is the extension ratio of the specimen at the onset of crack propagation. Hence, values of G_{Ic} were obtained from linear least-squares plots of $2kW_c$ versus a^{-1}, all of which were linear with correlation coefficients of ≥ 0.90, and values of 95% confidence limits typically ± 10%.

In order to provide limiting values of the respective fracture parameters, which are independent of the specimen geometry, the G_{Ic} analysis requires the specimens to be deformed under conditions of plane strain, such that the strain in the specimen normal to the applied stress is zero. Thus a thickness criterion must be met, which for specimens of thickness b is given by

$$b_{min} = 2.5(G_{Ic}E/\sigma_y^2) \quad (2)$$

The values of G_{Ic} derived from the SENT tests and the respective values of b_{min} are given in Table 5. The RIM mould used in these studies had a constant thickness of 3.5 mm and it can be seen that only for material M40 is the thickness of the specimens close to fulfilling the minimum thickness criteria. The values of G_{Ic} determined at a sample thickness $< b_{min}$ are not absolute due to a significant degree of plane stress behaviour, which results in an overestimation of the fracture parameters. However, they may be used in internal comparisons to show trends in RIM-copolymer fracture behaviour at a sample thickness of 3.5 mm, which is a common thickness for RIM mouldings. In general, the RIM-PU show significant increases in G_{Ic} with both HS content and SS-f_n. At 40% HS-content values of G_{Ic} are low, varying between 1.3 kJ m^{-2} for D40 and 0.6 kJ m^{-2} for M40. The latter value is, however, much greater than the value of 0.2 kJ m^{-2} reported [32] for the M1/MDI homopolyurethane network (i.e. HS% = 0). Thus, the HS-domains appear to generate a significant improvement in the fracture resistance of RIM-PU, and over the HS range studied G_{Ic} increased linearly with HS-content. In addition, the rate of increase of G_{Ic} with HS-content was greater the higher the SS-f_n, indicating a strong influence of copolymer molar mass on the fracture resistance of the RIM-PU.

3.7. Recursive method calculations

In an attempt to gain a better understanding of structure

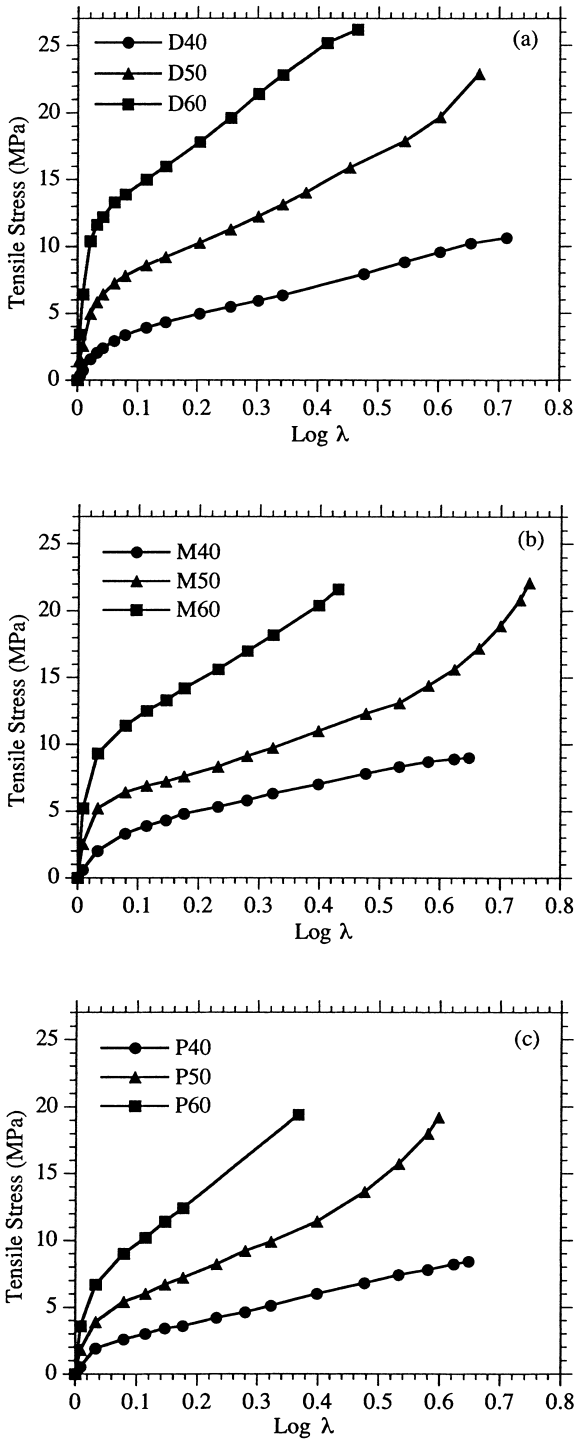

Fig. 3. Tensile stress–strain curves for copolyurethanes based on the soft-segment polyols (a) DS25, (b) M1 and (c) P1.

development during RIM-PU copolymerisations, the growth of weight-average copolymer molar mass (M_w) and hard segment sequence length (N_w), as functions of isocyanate conversion (p) were modelled using recursive-method calculations [36]. This is a simple method for calculating the average molar masses of polymers without first determining their distributions, and has been applied to linear [37,38] and non-linear [18,39] RIM-copolymerisations. The method utilises the recursive nature of a step-copolymerisation modelled as a first-order Markov chain process [40]. Thus, to determine weight-average molar mass in a typical three-component RIM system, a unit of each reactant is selected at random and the expected weight of the molecule of which it is a part is calculated; M_w is then obtained by averaging the weights of the three selected polymer molecules.

Recursive-method calculations were made for three-component $RA_2 + RB_2 + RC_f$ systems (diisocyanate/chain extender/prepolymer), corresponding to copolymers comprising 40, 50 and 60% (w/w) ED/MDI HS and a SS-prepolymer of $E_n = 2000\ g\ mol^{-1}$ and $f_n = 2$, 3 or 4. Assumptions used in the modelling are that homogeneous reaction conditions exist, that all groups react independently of each other, that the diisocyanate and chain extender are di-functional and that the ratio of the rate constants, K, (isocyanate-SS: isocyanate-chain extender) is equal to 1 and is independent of temperature and conversion. As in previous studies [18,37,38], overall second order kinetics were assumed. Kinetics equations were solved numerically to determine the conversion of each reactant as a function of time which, when coupled with the recursive method calculations, allowed the calculation of M_w and N_w as functions of isocyanate conversion (p).

The development of M_w for RIM-PU of 40, 50 and 60% HS-content is shown in Fig. 4(a)–(c), respectively. In each case, the curves initially show little increase in M_w, as reactions of the diisocyanate act mainly to produce low molar mass HS oligomers and to end-cap the polyol SS-prepolymer. However, as the reaction proceeds the SS-prepolymer molecules become linked, as AB block copolymer structures form, and M_w increases more rapidly. On increasing the functionality of the SS-prepolymer from 2 to 4 the development of copolymer structure (and the rapid upturn in M_w) occurs at lower values of p. For example, in Fig. 4(b) the upturn in M_w begins at values of p of approximately 0.5, 0.6 and 0.7 as the functionality of the SS-prepolymer increases from 2 to 3 to 4, respectively. For systems based on SS-prepolymers with a functionality >2, increasing the HS-content effectively reduces the functionality of the SS-prepolymer/chain extender mixture. The effect of HS-content is illustrated more clearly in Fig. 5, in which the development of M_w is shown for the three P1-based systems. Thus, as HS-content increases the upturn in M_w is shifted from $p \approx 0.5$ (P40) to $p \geq 0.6$ as a result of the reduction in functionality of the reaction mixture.

The conversions of isocyanate at gelation, p_g, were calculated for the non-linear systems using:

$$(rp_g)^2 = \frac{1}{(f_e - 1)(g_e - 1)} \tag{3}$$

where r is the stoichiometric ratio and $f_e = \Sigma f_i^2 A f_i / \Sigma f_i A f_i$ is the weight average functionality of a mixture of i various

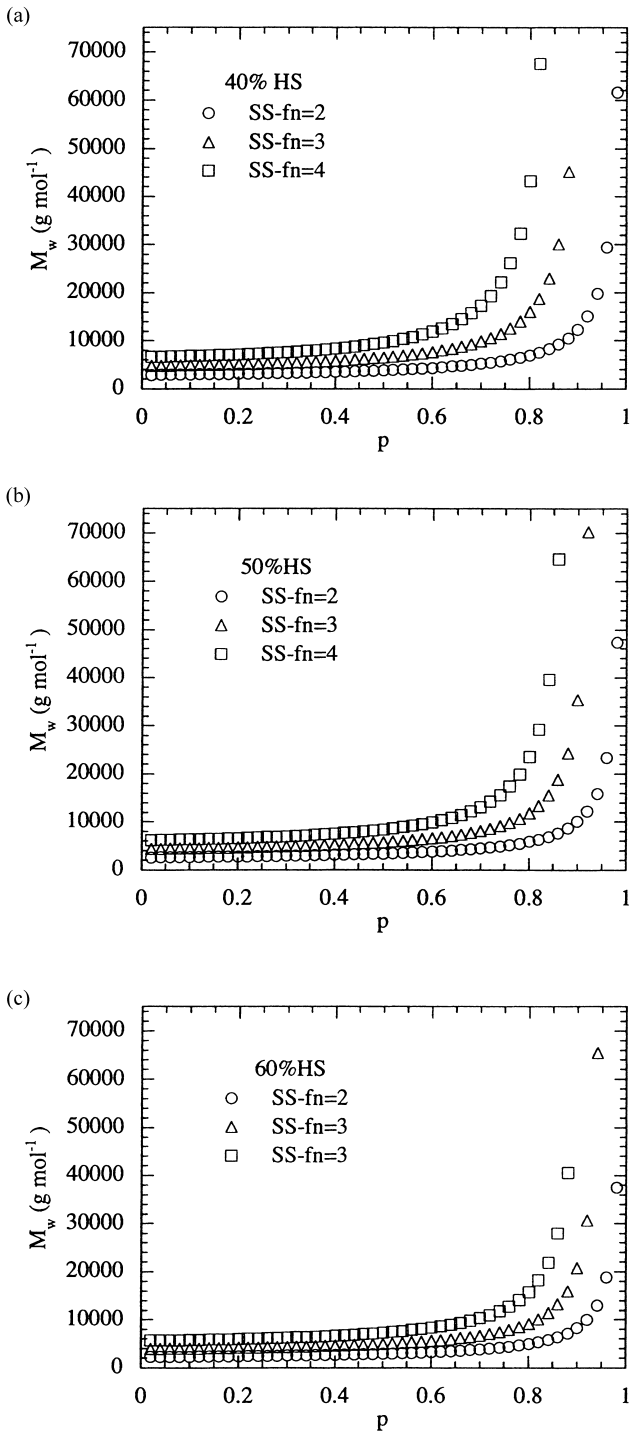

Fig. 4. The development of weight-average molar mass as a function of isocyanate conversion (p) during RIM-copolymerisation. M_w data have been predicted by recursive-method calculations. The compositional parameters used in the calculations correspond to (a) 40, (b) 50 or (c) 60% HS content copolyurethane comprising MDI, ED and SS-prepolymers with equivalent weight 2000 g mol^{-1} and SS-f_n of 2, 3 or 4.

SS-prepolymers and chain extenders with molar concentration Af_i; g_e is defined similarly for the isocyanates [1]. Using values of $f_n = 2$ for ED and MDI and a value of SS-prepolymer f_n of 4 the levels of p_g calculated for the P1-based systems range from 0.70 to 0.76 to 0.82 as HS content increases from 40 to 60%. However, the polyisocyanate and polyols used in this study have values of functionality which differ from these nominal values and values of p_g calculated for the RIM-PU, using experimental data for the reactants described in Table 2, range from 0.83 ± 0.02 (P1-based systems) to 0.87 ± 0.01 (M1-based systems) to 0.90 (DS25-based systems). Thus, since copolymerisation is effectively quenched at a relatively early stage by the onset of HS solidification, chemical gelation is not envisaged to have occurred, although the network-forming reactions obviously have a significant affect on the development of M_w.

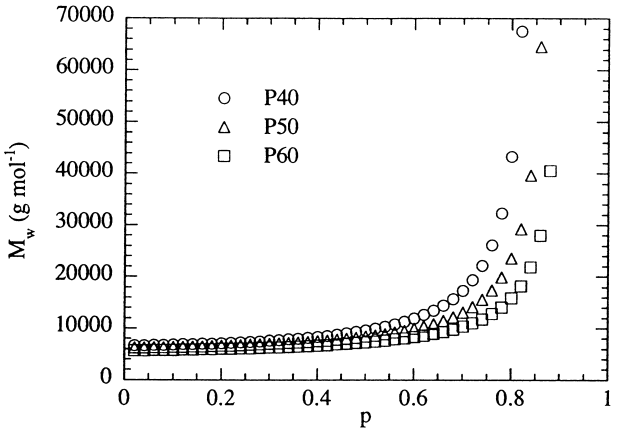

Fig. 5. The development of weight-average molar mass as a function of isocyanate conversion (p) during RIM-copolymerisation for systems based on the SS-prepolymer P1 with equivalent weight of 2000 g mol^{-1} and a SS-f_n of 4.

Variations of SS-prepolymer functionality (at constant E_n) have no effect on the development of N_w during copolymerisation; thus the recursive-method calculations generate only a single set of curves (Fig. 6) at various values of HS-content for the three theoretical systems. Only relatively small differences are observed in the development

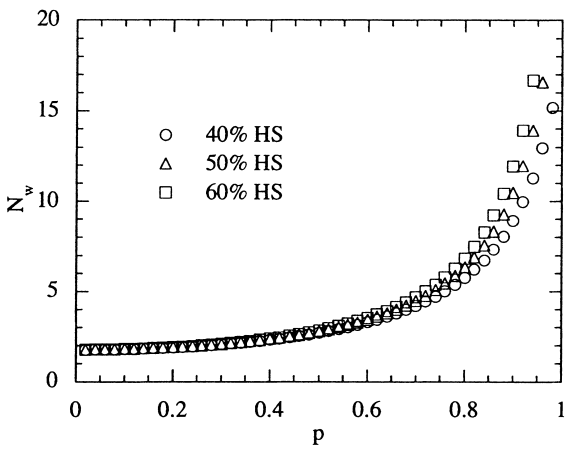

Fig. 6. The development of weight-average HS sequence length (N_w) as a function of isocyanate conversion (p) during copolymerisation of RIM-PU of varying HS content (40, 50, 60% by weight) as predicted by recursive-method calculations.

of HS sequence lengths in the RIM-PU until values of p exceed ~0.8. The model therefore proposes that copolymers contain longer HS-sequence lengths at higher HS-contents, and should therefore exhibit higher values of T_g^H. However, as copolymerisation is effectively quenched at a relatively early stage differences in N_w may be small. The DMTA data presented earlier (Table 4 and Figs. 1 and 2) did show significant differences in T_g^H between the RIM-PU systems, with the 40% HS materials exhibiting no obvious glass transitions whereas the 50 and 60% HS materials exhibited transition peaks at ~130 °C, which increased in intensity with increasing HS-content suggesting the presence of longer HS sequence lengths.

4. Conclusions

During RIM-copolymerisation of PU, significant variations in the development of molar mass occurred. These variations were due either to changes in SS-f_n or in the HS-content of the RIM-PU, both of which markedly affected the development of copolymer structure as the reacting system phase separated via spinodal decomposition. A statistical model of the copolymerisation, based on recursive-method calculations, showed that both higher SS-f_n and lower HS-content resulted in a more rapid development of copolymer molar mass. Consequently, increasing SS-f_n was shown to reduce the overall degree of phase separation developed in these materials (as determined by DSC and DMTA), due to increased domain boundary mixing. In contrast, increasing the HS-content from 40 to 60% was found to result in a decrease in the overall degree of phase separation. This is a consequence of the dynamic nature of the RIM process, as the onset of microphase separation occurs at an earlier stage of the copolymerisation for systems of higher HS-content.

The RIM-PU exhibited a wide range of mechanical behaviour resulting from structural variations in these multiphase materials; namely, HS-content, copolymer molar mass (i.e. changing SS-f_n) and the degree of phase separation. As expected, tensile properties were found to be dominated by HS-content, with the HS phase acting to significantly reinforce a relatively weak polyether elastomer phase. Consequently, the decrease in the degree of phase separation resulting from increasing SS-f_n lead to a general reduction in tensile properties. Fracture properties were also found to improve significantly with increasing HS-content. However, in contrast to tensile behaviour, the rate of increase in G_{Ic} with HS-content was greater the higher the SS-f_n, indicating a strong influence of copolymer molar mass on the fracture resistance of the RIM-PU.

References

[1] Macosko CW. Fundamentals of reaction injection moulding. Munich: Hanser; 1989.
[2] Ryan AJ. Polymer 1990;31:707–12.
[3] Hamley IW, Stanford JL, Wilkinson AN, Elwell MJ, Ryan AJ. Polymer 2000;41:2569–76.
[4] Teixeira PIC, Read DJ, McLeish TCB. Macromolecules 2000;33:3871–8.
[5] Ryan AJ, Stanford JL, Still RH. Polymer 1991;32:1426–39.
[6] Ryan AJ, Stanford JL, Birch AJ. Polymer 1993;34:4874–81.
[7] Macosko CW. Fundamentals of reaction injection moulding. Munich: Hanser; 1989. section 2.7.
[8] Stanford JL. In: Stepto RFT, editor. Polymer networks—principles of formation, structure and properties. London: Blackie; 1997. Chapter 5.
[9] Camberlin Y, Pascault JP. J Polym Sci, Polym Phys Ed 1984;22:1835–44.
[10] Ryan AJ, Stanford JL, Still RH. Polym Commun 1988;29:196–8.
[11] Critchfield FE, Gerkin RM. J Elast Plast 1976;8:396–402.
[12] Zdrahala RJ, Hager SL, Gerkin RM, Critchfield FE. J Elast Plast 1980;12:225–44.
[13] Camargo RE, Macosko CW, Tirrell M, Wellinghoff ST. Polymer 1985;26:1145–54.
[14] Nishimura H, Kojima H, Yarita T, Nishiro M. Polym Engng Sci 1986;26:585–92.
[15] Markovs RA. J Cell Plast 1985;326–31.
[16] Burchell DJ, Porter R. Proc '32nd SPI Ann PU Tech Mark Conf 1989;144–8.
[17] Morgan RE, Berg JW, Klumb GA. Proc 32nd SPI Ann PU Tech Mark Conf 1989;262–8.
[18] Stanford JL, Still RH, Wilkinson AN. Polymer 1995;36:3555–64.
[19] Galla EA, Mascioli RL, Bechara IS. J Elast Plast 1981;13:205–23.
[20] Wilkinson AN. PhD Thesis. Victoria University of Manchester; 1990.
[21] Camberlin Y, Pascault JP. J Polym Sci, Polym Chem Ed 1983;21:415–23.
[22] Saunders JH, Frisch KC, Polyurethanes chemistry and technology part 1, New York: Interscience; 1962. p. 32–6.
[23] Woods G. The ICI polyurethanes book, 2nd ed. London: ICI/Wiley; 1990. p. 35–9.
[24] Glasspool J. Proc. of UTECH 86, The Hague, The Netherlands 1986;14–19.
[25] Yang WP. PhD Thesis. University of Minnesota; 1987.
[26] Macosko CW. Fundamentals of reaction injection moulding. Munich: Hanser; 1989. section 6.3.
[27] Leibler L. Macromolecules 1980;13:1602–17.
[28] Benoit H, Hadziannou G. Macromolecules 1988;21:1449–64.
[29] Ryan AJ, Willkomm WR, Bergstrom TB, Macosko CW, Koberstein JT, Yu CC, Russell TP. Macromolecules 1991;24:2883–9.
[30] Elwell MJ, Mortimer S, Ryan AJ. Macromolecules 1994;27:5428–39.
[31] Turner RB, Spell HL, Vanderhider JA. In: Kresta JE, editor. Reaction injection moulding and fast polymerization reactions. Polymer science and technology, vol. 18. New York: Plenum; 1982. p. 63–76.
[32] Lyne J. PhD Thesis. Victoria University of Manchester; 1990.
[33] Bengtson B, Feger C, MacKnight WJ, Schneider NS. Polymer 1985;26:895–900.
[34] Rivlin RS, Thomas AG. J Polym Sci 1953;10:291–9.
[35] Lake G. J Proc Yield Deform Fract Polym, Phys Inst, London 1970;531.
[36] Lopez-Serrano F, Castro JM, Macosko CW, Tirrell M. Polymer 1980;21:263–73.
[37] Pannone MC. MS Thesis. USA: University of Minnesota; 1985.
[38] Pannone MC, Macosko CW. Polym Engng Sci 1988;28:660–9.
[39] Wang KJ, Huang YJ, Lee LJ. Polym Engng Sci 1990;30:654–64.
[40] Flory PJ. Principles of polymer chemistry. Ithaca: Cornell Press; 1953. Chapter 3.